HOKKAIDO UNIVERSITY

Title	Effects of autoimmune abnormalities on skeletal muscle regeneration after needle puncture in mice
Author(s)	Masugi, Misato; Ichii, Osamu; Otani, Yuki et al.
Citation	Experimental biology and medicine https://doi.org/10.1177/15353702231198073
Issue Date	2023-09-26
Doc URL	https://hdl.handle.net/2115/90626
Type	journal article
File Information	108419.pdf

1 **Effects of autoimmune abnormalities on skeletal muscle regeneration after needle**

2 **puncture in mice**

3

4 **Short title**: Punctured muscle injury and regeneration in mice with autoimmune abnormalities

5

6 Misato Masugi[1], Osamu Ichii[1,2]*, Yuki Otani[1], Takashi Namba[1], and Yasuhiro Kon[1]

7

8 [1]Laboratory of Anatomy, Department of Basic Veterinary Sciences, Faculty of Veterinary

9 Medicine, Hokkaido University, 060-0818, Japan

10 [2]Laboratory of Agrobiomedical Science, Faculty of Agriculture, Hokkaido University, 060-

11 8589, Sapporo, Japan

12

13 **Corresponding author**: Osamu Ichii, D.V.M., Ph.D.

14 Laboratory of Anatomy, Department of Basic Veterinary Sciences, Faculty of Veterinary

15 Medicine, Hokkaido University, Kita 18-Nishi 9, Kita-ku, Sapporo, JAPAN.

16 Tel & Fax: +81-11-706-5188, Email: ichi-o@vetmed.hokudai.ac.jp

17

18

19   **Abstract**

20   Regeneration of injured skeletal muscles is supported by the activation of satellite cells, and

21   excessive traumatic injuries may trigger abnormal processes, such as fibrosis. Because the

22   participation of immune cells is crucial during skeletal muscle repair, systemic autoimmune

23   diseases impair their regeneration. This study focused on a traumatic injury by injection and

24   investigated the effect of autoimmune diseases on skeletal muscle regeneration. Male mice of

25   MRL/MpJ-*Fas^{lpr/lpr}* and MRL/MpJ (6–7 months old) were used for autoimmune disease and

26   healthy groups. The abdominal walls punctured by a needle were histologically analyzed at 1,

27   3, and 8 days post-injection. In both groups, injured skeletal muscle tissues showed necrosis

28   and inflammatory cell infiltrations on day 1, increased cell density at 3 days, and regenerative

29   myotubes with central nuclei without fibrosis at 8 days. Gr-1$^+$ neutrophils at injured skeletal

30   muscle were abundant at 1 day, and then substantially decreased starting from 3 days in both

31   groups. The number of CD3$^+$ T cells was remarkably higher in MRL/MpJ-*Fas^{lpr/lpr}* than that in

32   MRL/MpJ at 1 day, and a similar tendency was observed in B220$^+$ B cells. The numbers of

33   IBA1$^+$ macrophages and bromodeoxyuridine-incorporating cells tended to be higher at 3 days,

34   and those of the latter, mainly proliferating paired-box-7$^+$ satellite cells, showed significance

35   at other time points and negatively correlated with the autoimmune disease indices, such as

36   spleen weights or serum autoantibody level. Thus, this result suggested that injured skeletal

37   muscle by minor trauma is normally regenerated regardless of the effects of autoimmune

38   diseases, although lymphocyte infiltrations during these processes were more severe in

39   MRL/MpJ-*Fas^{lpr/lpr}*.

40   **Keywords:** autoimmune disease, MRL/MpJ-*Fas^{lpr/lpr}*, skeletal muscle, injection, muscle

41   regeneration, histopathology

42

43 **Impact statement**

44 Mild traumatic injury of skeletal muscles is generally observed in the clinical field, such as

45 intramuscular injection, and is characterized by muscle regeneration after immune cell

46 infiltration. Therefore, autoimmune diseases could affect the repair process of traumatic

47 skeletal muscle injury, but their pathological modification has been unclear. This study

48 revealed the histopathological features of abdominal walls that received a needle puncture in

49 an autoimmune disease mouse model. Infiltrations of lymphocytes, particularly T cells,

50 around the injured muscle were substantially increased in mice with autoimmune disease.

51 However, these muscles were regenerated without any abnormalities, such as fibrosis, with

52 proliferation of fibro-adipogenic progenitors, in such mild injury. Therefore, this study

53 provided the basic knowledge to understand the process and features of muscle regeneration

54 in case of mild traumatic injuries in patients with autoimmune disease.

55

Introduction

Skeletal muscles continue regeneration and reconstruction to maintain their morpho-function during the lifetime. In a healthy status, skeletal muscles contain a pool of satellite cells, which are undifferentiated and quiescent mononuclear cells surrounding mature skeletal muscle cells. Their activation and differentiation are crucial for skeletal muscle regeneration accompanied by infiltrations of immune cells and activation of fibro-adipogenic progenitors (FAPs). FAPs are present in the skeletal muscle stroma, regulate immune cell accumulation and function, and influence the homeostasis of the satellite cell pool and myogenesis.[1] FAPs are not myogenic cells but have the bipotential abilities to differentiate into fibroblasts or adipogenic cells, and their cell fate is strongly affected by the external environment in the tissues.[2,3]

In a familiar environment, several skeletal muscle injuries are caused by accidents or medical treatments, such as surgery or intramuscular injection (i.m.). Generally, at the acute phase of traumatic skeletal muscle injury, myocytes undergo necrosis, and immune cells accumulate in response to skeletal muscle injury during the repair process. Neutrophils start to accumulate starting from 24 h after injury, followed by macrophage infiltration and satellite cell proliferation. From the data of a mouse model for severe traumatic skeletal muscle injury[4], C57BL/6 mice (B6) showed a predominant accumulation of CD11b-positive (CD11b$^+$) cells at 3 days after injury induced by cardiotoxin (CTX) injection into the anterior tibial and quadriceps muscles. In this model, CD3$^+$ T cells increased at the injury site, and their numbers were maintained until day 5 after injection. At that time point, macrophage infiltrations switched from an inflammatory M1 to an anti-inflammatory M2 phenotype, and satellite cell proliferation reached its peak. Then, immune cells decreased whereas satellite cells showed self-duplication or formed centronuclear myotubes Thus, the injured skeletal muscles were repaired by collaboration with the immune system.

On the other hand, several factors, such as genetic abnormalities, systemic diseases, and aging, cause the abnormalities of remodeling or regeneration, such as fibrosis, ossification, or adipogenesis in the skeletal muscle. For example, Schwartz-Jampel syndrome and muscular

84 dystrophy are associated with genetic traits and cause skeletal muscle degeneration and

85 abnormal regeneration.[5] Moreover, in traumatic skeletal muscle injury, in addition to a

86 persistent infiltration of inflammatory cells, FAPs may proliferate and induce fibrosis,[6] even

87 though they would normally trigger apoptosis. Therefore, traumatic injuries by medical

88 treatments also induce the abnormalities of remodeling or regeneration in skeletal muscles. In

89 medical settings, advances in acute care and traumatic surgery have increased the

90 opportunities for medically induced traumatic skeletal muscle injuries. For example, surgical

91 trauma to the jaw, such as bone resection, intramuscular injection, dental treatment, or

92 surgery, is the most common cause of heterotopic ossification of the masticatory muscles and

93 may cause deformity of the jaw joint.[7] Autoimmune diseases (AIDs) are characterized by the

94 production of autoantibodies or autoreactive cells in response to tissues. The number of

95 patients with AIDs is increasing each year.[8] Because skeletal muscle regeneration is related to

96 the immune system, their abnormalities might be closely associated. Idiopathic myositis is an

97 AID that targets skeletal muscle and is characterized by weakness, inflammation, and fibrosis

98 of skeletal muscles.[9] On the other hand, the pathological correlation between autoimmune

99 abnormalities and traumatic skeletal muscle injury remains unclear.

100   The pathological crosstalk between the immune system and skeletal muscle was mainly

101 examined by using severe experimental models induced by i.m. of myopathic reagents, such

102 as CTX;[10] however, few studies have examined this crosstalk in milder skeletal muscle injury.

103 In this study, we focused on needle puncture as a traumatic skeletal muscle injury and

104 investigated the relationship between skeletal muscle remodeling or regeneration and

105 autoimmune abnormalities by using a mouse model. The results obtained from the present

106 study revealed the effects of mild traumatic skeletal muscle injury on mice with healthy or

107 autoimmune abnormalities. Therefore, this study provides crucial insight into evaluation of

108 the effects of universally practiced medical treatments, particularly skeletal muscle needle

109 puncture.

Materials and methods

Animals

Male MRL/MpJ (MpJ), MRL/MpJ-*Fas^{lpr/lpr}* (lpr), and B6 mice were purchased from Japan

SLC, Inc. (Hamamatsu, Japan) and maintained under specific pathogen-free conditions.

Animal experimentation was approved by the Institutional Animal Care and Use Committee

of the Faculty of Veterinary Medicine, Hokkaido University (approval No. 21-0008). All

experimental animals were handled by the Guide for the Care and Use of Laboratory Animals,

Faculty of Veterinary Medicine, Hokkaido University (approved by the Association for

Assessment and Accreditation of Laboratory Animal Care International).

Preparation of the abdominal wall puncture model

At 6–7 months of age, mice were weighed and anesthetized by intraperitoneal injection (i.p.)

of a mixture of medetomidine (0.3 mg/kg), midazolam (4 mg/kg), and butorphanol (5 mg/kg)

from the left area of the abdominal wall. Then, the abdominal skin was shaved and

disinfected, and mice were gently kept warm and recovered by administering atipamezole (0.3

mg/kg, i.p.) with a 21G needle from the right-side abdominal wall. Then this area was

recorded as a needle puncture site. Mice were euthanized 1, 3 or 8 days after the needle

puncture, and tissue samples were collected (Figure 1A). All mice were administered

bromodeoxyuridine (BrdU) (1 mg/10 g body weight (BW), i.p.) 2-3h before they euthanized.

Euthanasia was performed by cutting the femoral artery and dislocating the cervical vertebrae

under deep anesthesia. The abdominal wall, including the external and internal oblique

abdominal muscle and the transverse abdominis muscle, was collected without distinction

because they were difficult to separately isolate. The right part of abdominal wall was used as

the needle puncture site. Subsequently, the spleens were immediately collected and weighed.

Serological analysis

For an index of AID development, serum levels of anti-double-stranded DNA (dsDNA)

antibodies were measured to evaluate systemic autoimmune conditions using LBIS anti

6

138 dsDNA-mouse ELISA kit (FUJIFILM Wako Pure Chemical Corporation; Osaka, Japan)

139 according to manufacturer's instructions. As another index, the ratio of the spleen weight

140 (SPW) to BW (SPW/BW) was calculated.

141

142 ***Histological analysis***

143 Needle puncture was performed perpendicular to the abdominal wall muscle, and the entire

144 abdominal wall, including the punctured area, was subsequently collected. The abdominal

145 wall was then stretched onto a flat surface, fixed in 4% paraformaldehyde overnight at 4 °C,

146 and embedded in paraffin. Longitudinal sections (3–4-μm thick) were cut through the

147 abdominal wall muscle; each section therefore contained a transverse cross-section of the

148 punctured area. Deparaffinized sections were stained with hematoxylin-eosin (HE) or Elastica

149 van Gieson (EVG), and The punctured area was identified by observing injured muscles.

150

151 ***Immunohistochemistry (IHC) and immunofluorescence (IF)***

152 IHC for IBA1, Gr-1, B220, CD3, and BrdU was performed to detect the macrophages,

153 neutrophils, B cells, T cells, and proliferating cells, respectively. Briefly, paraffin sections

154 were deparaffinized, and antigen was retrieved by heating. Then, to block internal peroxidase

155 activity, the sections were soaked in methanol containing 0.3% H_2O_2 for 20 min at 25 °C.

156 After washing 3 times in phosphate-buffered saline (PBS), the sections were incubated with a

157 blocking serum for 1 h at room temperature to block non-specific reactions. Then, sections

158 were incubated with primary antibodies overnight at 4 °C. After washing 3 times in PBS, the

159 sections were incubated with secondary antibodies for 30 min at 25 °C and washed 3 times in

160 PBS. Consequently, the sections were incubated with streptavidin-conjugated horseradish

161 peroxidase (SABPO® kit, Nichirei; Tokyo, Japan) for 30 min at 25 °C, washed 3 times in

162 PBS, and the immunopositive reaction was visualized with 10 mg of 3,3'-diaminobenzidine

163 tetrahydrochloride in 50 mL 0.05 M Tris-H_2O_2 solution. Finally, the sections were

164 counterstained with hematoxylin. The details of the antibodies, antigen retrieval, and blocking

165 are listed in Table 1.

166   IF was performed to detect BrdU-incorporating cells and positive cells for paired box 7

167   (PAX7) or platelet-derived growth factor receptor α (PGDFRα). The paraffin sections were

168   deparaffinized, subjected to antigen retrieval, and then blocked using normal donkey serum,

169   using the same protocol as that for IHC. After overnight incubation with the primary

170   antibodies, sections were incubated with the secondary antibody for 1 h at 25 °C. The sections

171   were sealed with a water-soluble encapsulant and observed under fluorescence microscopy

172   (BZX-710; Keyence; Osaka, Japan). The details of antigen retrieval, dilution, and source of

173   antibodies are listed in Table 1.

174

175   *Histoplanimetry*

176   IHC sections were converted to virtual slides by Nano Zoomer 2.0 RS (Hamamatsu Photonics

177   Co., Ltd.; Hamamatsu, Japan). Using NDP view2 (Hamamatsu Photonics Co., Ltd.), 3–5

178   images of the puncture site were randomly selected at 40× magnification. Then, the number of

179   total and positive cell nuclei in necrotic areas was manually identified in the IHC-stained

180   images of IBA1, Gr-1, B220, CD3, and BrdU. Each percentage of the number of positive cell

181   nuclei to total cell nuclei in the injury region was calculated. Because of the strong

182   nonspecific response of IBA1 to necrotic cytoplasm, BZ-X710 and BZ-H3C (Keyence) color

183   discrimination was used to identify positive cells.

184

185   *Statistical analysis*

186   The results were expressed as the mean ± standard error (SE) and analyzed by non-parametric

187   statistical methods. Significant difference between 2 groups was assessed by Mann-Whitney

188   *U* test. Kruskal-Wallis test was used to compare the numerical results, and multiple

189   comparisons were performed using Dunnett's test when significant differences were observed.

190   The correlation was analyzed using Spearman's correlation test. A *P* value lower than 0.05

191   was regarded as a significant difference in all analyses. All statistical analysis was performed

192   using IBM SPSS ver. 28.0.1 (IBM Japan Ltd., Tokyo, Japan)

193 **Results**

194 ***Indices of AID***

195 According to Figure 1A, treatment and sampling were performed at 1, 3, and 8 days. Serum

196 levels of anti-dsDNA antibody and the ratio of SPW/BW of 6–7-month-old MpJ and lpr mice

197 were measured at each time point as indices of AID (Figures 1B and C). Lpr mice showed

198 significantly higher values compared with those of MpJ mice in both indices at all time points

199 (note logarithmic display). Furthermore, MpJ mice at 8 days and lpr mice at 3 days showed

200 significantly higher serum levels of anti-dsDNA antibody compared to each value at 1 day.

201 These data indicated that the lpr mice used in this experiment developed a systemic AID.

202

203 ***Histological alterations of the puncture region over time***

204 As shown in the images of HE-stained section from MpJ at 1 day (Figure 2A), the injured

205 myofibers at the puncture region showed necrosis and a paler color compared with that of the

206 surrounding intact myofibers. These alternations were observed along with the longitudinal

207 axis of injured myofibers and separated the injured and healthy skeletal muscle tissue.

208 Therefore, these necrotic areas were defined as the injured area surrounded by healthy

209 myofibers.

210 　　Figure 2B shows the HE-stained cross sections of the abdominal wall muscle, including

211 the injured area, and summarizes the histological alternations of MpJ and lpr mice during the

212 observation period. Briefly, MpJ and lpr mice showed similar histological alterations. On day

213 1, the injured myofibers were necrotic with a few scattered infiltrations of inflammatory cells

214 and blood cells. On day 3, abundant mononuclear cell infiltrations were observed between the

215 necrotic myofibers, indicating induction of local inflammatory response. On day 8, the

216 number of infiltrating cells decreased, and many regenerative myotubes with central nuclei

217 were observed. Thus, comparable histological changes in the injury and regenerative process

218 of skeletal muscles by needle puncture were observed, and the features of inflammatory

219 response at 3 days and regeneration at 8 days were prominent in both strains.

220

221   *Inflammatory cell infiltration at the puncture region*

222   Next, we assessed macrophages and neutrophils, which are known to be initially induced in

223   the region of skeletal muscle injury.[11] Moreover, B and T cells were examined to evaluate

224   their relationship with AIDs.

225   As shown in Figure 3, IBA1$^+$ macrophages were abundantly observed at 3 days among

226   all examined inflammatory cells in both strains and tended to be comparable or decreased at 8

227   days (Figure 3A). On the other hand, common to both strains, abundant Gr-1$^+$ neutrophils

228   were observed at 1 day and decreased onward (Figure 3B). Quantification of these

229   inflammatory cells showed that IBA1$^+$ macrophages exhibited the highest values at 3 days in

230   both strains without strain- or time course-related significant differences (Figure 3C). For Gr-

231   1$^+$ neutrophils, the quantitative values at 1 day were significantly higher than those at other

232   time points in both strains without strain differences (Figure 3D).

233   As shown in Figures 4A and B, the number of lymphocytes was lower than that of

234   macrophages and neutrophils, but some differences were detected between studied strains.

235   Briefly, the quantification of these cells showed no change in B220$^+$ B cells of MpJ mice

236   during the observation periods, but lpr mice showed the highest values at 1 day with a higher

237   tendency compared with that of MpJ (P=0.063) and then decreased (Figure 4C). Similar

238   tendency was also observed in CD3$^+$ T cells, and lpr mice showed a significantly higher value

239   compared with that of MpJ at 1 day and then decreased (Figure 4D). Thus, lpr mice were

240   suggested to induce more lymphocyte infiltration among injured myofibers at 1 day compared

241   with that of MpJ mice.

242

243   *Proliferating cells at the puncture region*

244   During skeletal muscle regeneration, the formation of myotubes by proliferation,

245   differentiation, and fusion of satellite cells is important.[12]

246   Figure 5A shows the IHC images of BrdU-incorporating proliferating cells in the

247   puncture region of MpJ and lpr mice. Few positive cells were detected at 1 day in both strains,

248   but they were observed as numerous at 3 days and tended to decrease at 8 days.

249   Quantification of BrdU-incorporating cells (Figure 5B) showed that the values in MpJ were

250   significantly higher at 3 days compared with those at 1 and 8 days. Lpr mice also showed a

251   similar tendency, and a significant difference was observed between 1 and 3 days. Further, the

252   values at 3 days tended to be higher in MpJ than those in lpr mice (P=0.095).

253   Next, the cell type of BrdU-incorporating cells was investigated by assessment of IF.

254   PAX7 and PDGFRα, which were used as markers for satellite cell activation from quiescent

255   to proliferative stages and for FAPs, which are mesenchymal progenitor cells known to

256   influence myogenesis by regulating immune cell accumulation and function and by providing

257   extracellular matrix components.[2,13] In both strains, almost all PAX7+ nuclei showed the

258   merged reactions with BrdU-incorporating nuclei during the observation period (Figures 5C).

259   On the other hand, PDGFRα+ cells rarely showed BrdU incorporation (Figures 5C). This

260   suggests that many satellite cells have been activated from the quiescent to the proliferative

261   phase at the 3 days injury region.

262   To confirm the influence of the genetic background of the mice, the same experiment

263   was conducted with B6 mice (Supplemental figure 1). We found that all BrdU-incorporating

264   nuclei observed were PAX7+ nuclei at 3 days, similar to MpJ and lpr mice.

265

266   ***Verification of fibrosis as a regenerative abnormality***

267   Finally, to examine the fibrosis associated with the skeletal muscle injury, EVG-stained

268   sections were observed. Figure 6 shows EVG-stained cross sections of the abdominal wall

269   muscle, including the injured area, and summarizes the histological alterations over time in

270   MpJ and lpr mice. At 1 day, it showed a decrease in the staining intensity of picric acid+

271   myofibers at the injury region owing to necrosis, and a very small amount of collagen fibers

272   were observed in the interstitium of the skeletal muscles. At 3 days, there was a notable

273   increase in collagen fibers, and the necrotic tissue showed abundant cells, including

274   infiltrating cells. However, at 8 days, when skeletal muscle regeneration was initiated,

275   centronuclear myocytes (as shown in Figure 2B) were formed similarly to normal myofibers,

276   and a significant decrease in collagen fibers was observed, confirming a smooth regeneration

11

277   process. Thus, in both strains, no fibrotic features were detected in the injury region,

278   indicating normal regeneration of skeletal muscles.

279

280

Discussion

This study aimed to clarify the effects of systemic immunological abnormalities on the repair processes of injured skeletal muscles. In particular, the authors focused on traumatic skeletal muscle injuries that are universally caused by medical treatments, such as i.m. The skeletal muscles of abdominal walls in AID-prone lpr mice were punctured. Their histological alterations with immunological indices at several time points were compared with those of MpJ, a healthy control strain of lpr mice. Although both strains showed similar skeletal muscle injuries and regeneration without fibrotic features, several features, such as lymphocyte infiltration dynamics, were different in these processes.

Several studies using mouse models with CTX- or glycerol-induced muscle injuries indicated that satellite cell activation continued up to day 4 after injury, myotubes with central nuclei were evident at day 7, and the diameter of these myotubes continued to increase until day 14.[14] In particular, the CTX model is suitable for studying uniform and complete regeneration. Fibrosis is mild and transient, and the CTX model is used globally. On the other hand, experimental glycerol myopathy could be a suitable model to study the pathophysiology of Duchenne muscular dystrophy, where impaired regeneration is observed, and fibrosis occurs. In the present study, we focused on needle puncture as a traumatic skeletal muscle injury and investigated the relationship between the remodeling or regeneration of skeletal muscle and autoimmune abnormalities by using a mouse model; therefore, we compared the result from CTX-model with our obtained data.

In the present study, sampling points were scheduled at day 1 (immediately after injury/acute inflammation), day 3 (active inflammation), and day 8 (regeneration) to elucidate the effects of AID on muscle injury inflammation and regeneration, with a particular focus on the cells localized to puncture lesions. Although fibrosis starts at day 4 due to the proliferation of fibroblasts in more severe cases,[14] no significant collagen deposition was noted in our model on day 3 and 8 after puncture. Furthermore, on day 8, there was no significant difference in the regeneration features (see Figures 2, 5, 6). Therefore, we concluded that fibrosis, as indicated by the proliferations of PDGFRα+ cells, did not occur in both healthy

13

309 <mark>and AID groups in this puncture model.</mark>

310   For examined indices of autoimmune abnormalities, the serum level of anti-dsDNA antibody

311 was gradually and significantly increased in MpJ mice from 1 to 8 days, and this increase was

312 more prominent in lpr mice from 1 to 3 days. For supportive data, correlation analysis was

313 performed between indices of AID and the quantitative values of examined cells (Supplemental

314 table 1). Although no significant correlation was observed within each group, the numbers of

315 $CD3^+$ T cells and $B220^+$ B cells temporarily increased at 1 and 3 days, respectively, when the

316 serum level of the anti-dsDNA antibody increased. This result was observed using all groups.

317 Myositis autoantigens, such as histidyl tRNA synthetase, Mi-2, U1-70kD, Ku/the catalytic

318 subunit of DNA-dependent protein kinase, are expressed at high levels in myositis skeletal

319 muscles, whereas they are very low in normal skeletal muscles; their expressions are

320 increased in cells that have features of regenerating skeletal muscle cells.[15] Furthermore,

321 traumatic skeletal muscle injury stimulates the production of autoantibodies following

322 inflammation.[16] Therefore, the authors supposed that lpr mice also developed myositis with

323 the increase of serum autoantibodies, such as an anti-dsDNA antibody, by the increase of this

324 autoantigen expression after skeletal muscle injuries. However, the myositis feature was not

325 clearly observed in lpr mice, and the skeletal muscle inflammation was mild and limited in a

326 locally injured area and eventually diminished at 8 days. Therefore, AID-prone mice induced

327 the production of anti-dsDNA antibodies more abundantly compared with that in healthy ones

328 after skeletal muscle injuries although they did not develop myositis. Furthermore, the authors

329 assumed that the pathological effects on systemic organs by autoantibody increase might be

330 mild after local traumatic skeletal muscle injury because no significant alteration was detected

331 in the ratio of SPW/BW from 1 to 3 days in both strains.

332   Traumatic skeletal muscle injuries in both strains resulted in infiltration of immune cells

333 that contribute to innate immune responses, such as neutrophils and macrophages. However, it

334 was characterized by a more abundant infiltration of lymphocytes, especially T cells, in lpr

335 mice. T cells ($CD45^+$ $CD11b^-$ $CD3^+$ cells) infiltrate the skeletal muscle after injury, and their

336 number in the skeletal muscle peaked at 3 days and remained constant through 5 days before

14

declining at 7 days by one CTX injection to the anterior tibialis and quadriceps muscles of 8–

10-week-old female B6 mice. Furthermore, it was suggested that they activated T helper cells,

consistently expressing CD4 but not CD8 marker.[4] Importantly, lpr mice developed

progressive lymphadenopathy after 6 weeks of age owing to accumulation of an abnormal

population of CD4⁻ CD8⁻ double negative T cells.[17,18] It is unclear whether these lymphocytes

in lpr mice recognized specific antigens derived from the destroyed myocytes or this was the

result of a nonspecific immune response; however, the lpr mutation itself and/or the

associated autoimmune abnormalities would affect the infiltration of lymphocytes, especially

T cells, at the injured skeletal muscle area.

Many myogenic progenitor cells and FAPs were detected as BrdU-incorporating cells at

3–4 days during the regeneration process after extensive skeletal muscle disruption with CTX

i.m. to the hindlimbs of B6 mice.[3] FAPs are quiescent in intact skeletal muscle but proliferate

in response to skeletal muscle injury to stimulate activation and differentiation of satellite

cells.[3,19,20] Therefore, in this study, PAX7⁺ satellite cells and PDGFRα⁺ FAPs were co-stained,

but only the formers proliferated at the injury site after puncture in both groups. Considering

the influence of the genetic background of the mice on this phenotype, the same experiments

were conducted with B6 mice (Supplemental figure 1); the results showed that, similar to MpJ

and lpr mice, all BrdU-incorporating cells were satellite cells, and FAPs did not show

incorporation. Therefore, it was concluded that FAPs activation is not induced in skeletal

muscle injury by puncture, although satellite cells locally proliferate. Regarding the

differences from previous studies using the CTX i.m. model,[3,19,20] the variation in the degree

of skeletal muscle injury, rather than the genetic background of the mice, was considered to

affect the proliferation kinetics of satellite cells and FAPs.

In healthy skeletal muscle tissue, satellite cells go from a quiescent state to a

proliferative phase a few days after injury and simultaneously start to repair the injured and

necrotic sites.[3,21] Increased proliferating cells at the injury site at 3 days tended to be less in

lpr than those in MpJ mice. Importantly, the autoantibody concentration of healthy MpJ mice

progressively increased up to 8 days. Because the majorities of the proliferating cells are

satellite cells, the change in MpJ autoantibody concentration may have reflected a transient

increase in regenerating myocytes expressing autoreactive autoantigen.[14,22] On the other hand,

at 3 days, lpr tended to have the same or fewer proliferating cells as those in MpJ mice, and

correlation analysis of all mice showed a negative correlation between the index of AID and

the number of proliferating cells. However, the increased autoantibody concentration at 3 days

was more remarkable in lpr than that in MpJ mice, suggesting that this phenotype reflects

excessive activation of the immune system to recognize the autoantigen rather than the

amount of autoantigen derived from the regenerating myocytes.[23] In addition, satellite cells

and FAPs in healthy skeletal muscle tissue distant from the injury site were compared

between MpJ and lpr mice, but no difference was detected in their number or localization

(data not shown).

Both strains had no remarkable fibrosis findings at the injury site. Essentially, fibrosis

occurs in damaged skeletal muscle when persistent inflammatory cell infiltration and fibroblast

activation produce a mass of nonfunctional fibrous tissue.[24,25] Apoptosis of FAPs is required for

normal skeletal muscle regeneration and the failure of apoptosis leads to skeletal muscle fibrosis

by increasing the survival rate of FAPs.[19,20] On the other hand, in this study, neither proliferation

of FAPs nor fibrosis were detected. Thus, it can be assumed that AIDs affect lymphocyte

induction and satellite cell dynamics in the early stages of injury, whereas minor skeletal muscle

injuries, such as puncture, do not directly lead to fibrosis or other regenerative abnormalities.

In conclusion, this study demonstrated that autoimmune abnormalities modified the

processes of inflammation and repair after skeletal muscle injury, whereas the skeletal

muscles injured by mild trauma, such as needle puncture can be normally regenerated. This

might suggest that the induction of immune-associated abnormal skeletal muscle regeneration

is affected by the kinds of reagents or adjuvants rather than the puncture itself, whereas the

accumulation of data from various conditions and diseases would be crucial. The obtained

results also emphasized an important perspective for future studies, especially focusing on the

significance of less invasive medical treatment for patients with autoimmune abnormalities.

Limitations

This study did not address the long-term effect of muscle puncture on AID status. Furthermore, a future study into how muscle-derived autoantigens influence systemic AID phenotypes would help comprehensively elucidate the effect of muscle puncture on AID and vice versa (e.g. muscle puncture before AID development at a young age, and analysis at 6–8 months of age using MRL/lpr) with functional effects, such as muscle contractility.

399 **Authors' contributions**

400 MM, OI, and YK designed and performed the experiments. MM, YO, and TN provided the

401 samples and analyzed the data. All authors were involved in writing the paper and have

402 approved the final manuscript.

403

Figure legends

Figure 1. Experimental schedule and indices for autoimmune abnormalities. (A) Experimental schedule. (B) The serum levels of anti-double-stranded DNA (dsDNA) antibody. (C) The percentage of spleen weight (SPW) to body weight (BW). The number of samples used is as follows: n=5 (MpJ/1 day), 4 (MpJ/3 days), 5 (MpJ/8 days), 4 (lpr/1 day), 4 (lpr/3 days), 4 (lpr/8 days). Each bar represents the mean ± SE. *: significant difference from the other strain at the same days that elapsed since puncture (Mann-Whitney U-test, *P<0.05). #: significant difference from the same strain at other days elapsed since puncture (Kruskal-Wallis test followed by Scheffé's method, #P <0.05). MpJ: MRL/MpJ, lpr: MRL/MpJ-$Fas^{lpr/lpr}$.

Figure 2. Histological features of myofibers in the injury region after needle puncture in the muscle. (A) Histological features of the abdominal wall muscle of MpJ mice at 1 day around the puncture region. The blue line represents the boundary between the injury and healthy regions. Myofibers at the injury region have necrotic cytoplasm. Bars=100 μm. *: Normal myofibers. (B) Histological alternations at the injury region of MpJ and lpr mice over time. Both strains show cellular infiltration owing to inflammatory response at 3 days. At 8 days, the number of infiltrating cells decreases, and many regenerative myotubes with central nuclei are observed (arrowheads). Insets indicate the squared area. Bars=100 μm. Hematoxylin-eosin staining. MpJ: MRL/MpJ, lpr: MRL/MpJ-$Fas^{lpr/lpr}$.

Figure 3. Infiltration of macrophages and neutrophils at the injury region after needle puncture in the muscle. (A) IBA1-positive macrophages (arrowheads). More cells are observed at 3 days in both strains. (B) Gr-1-positive neutrophils (arrowheads). More cells are observed at 1 day in both strains. Immunohistochemistry staining. Bars=100 μm. The blue line represents the boundary between the injury and healthy regions. (C) The percentage of the number of IBA1-positive cell nuclei to that of all cell nuclei in the injury region. (D) The percentage of the number of Gr-1-positive cell nuclei to that of all cell nuclei in the injury region. ND: Not detected. The number of samples used is as follows: n=5 (MpJ/1 day), 5

19

439   (MpJ/3 days), 5 (MpJ/8 days), 4 (lpr/1 day), 5 (lpr/3 days), 4 (lpr/8 days). Each bar represents

440   the mean ± SE. 3d, 8d: significant difference from the same strain at 3 days and 8 days since

441   puncture (Kruskal-Wallis test followed by Scheffé's method, [#]P <0.05). MpJ: MRL/MpJ, lpr:

442   MRL/MpJ-*Fas*[*lpr/lpr*].

443

444   **Figure 4. Infiltration of lymphocytes at the injury region after needle puncture in the**

445   **muscle.** (A) B220-positive B cells (arrowheads). Slightly more cells are observed in lpr at 1

446   day. (B) CD3-positive T cells (arrowheads). More cells are observed in lpr at 1 day.

447   Immunohistochemistry staining. Bars=100 μm. The blue line represents the boundary

448   between the injury and healthy regions. (C) The percentage of the number of B220-positive

449   cell nuclei to that of all cell nuclei in the injury region. (D) The percentage of the number of

450   CD3-positive cell nuclei to that of all cell nuclei in the injury region. The number of samples

451   used is as follows: n=5 (MpJ/1 day), 5 (MpJ/3 days), 5 (MpJ/8 days), 4 (lpr/1 day), 5 (lpr/3

452   days), 4 (lpr/8 days). Each bar represents the mean ± SE. *: significant difference from the

453   other strain at same days elapsed since puncture (Mann-Whitney *U*-test, *P <0.05). MpJ:

454   MRL/MpJ, lpr: MRL/MpJ-*Fas*[*lpr/lpr*].

455

456   **Figure 5. Proliferating cells in the injury region after needle puncture in the muscle.** (A)

457   Bromodeoxyuridine (BrdU)-incorporating cells (arrowhead). The blue line represents the

458   boundary between the injury and healthy regions. More cells are observed at 3 days in both

459   strains. Immunohistochemistry staining. Bars=100 μm. (B) The percentage of the number of

460   BrdU-incorporating cell nuclei to that of all cell nuclei in the injury region. The number of

461   samples used is as follows: n=5 (MpJ/1 day), 5 (MpJ/3 days), 5 (MpJ/8 days), 4 (lpr/1 day), 5

462   (lpr/3 days), 4 (lpr/8 days). Each bar represents the mean ± SE. 1d, 1d', 8d': significant

463   difference from the same strain at other days elapsed since puncture (Kruskal-Wallis test

464   followed by Scheffé's method, 1d P<0.05, 1d' 8d' P<0.01). Significant difference from the

465   other strain at same days are analyzed by Mann-Whitney *U*-test. (C) Double

466   immunofluorescence (IF) for BrdU (white/ proliferating cells) and paired box 7 (PAX7)

467 (red/satellite cells) or platelet-derived growth factor receptor α (PGDFRα) (green/ fibro-

468 adipogenic progenitors) at 3 days, 1 and 8 days. At 3 days, almost all BrdU-incorporating

469 cells are merged with PAX7-positive cells (arrowhead), not PGDFRα-positive cells (arrow) in

470 both strains. Similarly, at 1 and 8 days, both PAX7-positive cells and PDGFRα-positive cells

471 are localized at the injury region, and BrdU-incorporating cells merged with only PAX7 in

472 both strains. Blue: Hoechst (nuclei). Bars=100 μm. MpJ: MRL/MpJ, lpr: MRL/MpJ-*Fas$^{lpr/lpr}$*.

473

474 **Figure 6. Histological evaluation of fibrosis in the injury region after needle puncture in**

475 **the muscle.** Fibrosis of the abdominal wall muscle is examined at the injury region of MpJ

476 and lpr mice over time. No fibrotic features are detected in the injury region in both strains.

477 Collagen fibers are stained as purple. Elastica van Gieson staining. *(yellow): Normal

478 myofibers.. Bars=100 μm. MpJ: MRL/MpJ, lpr: MRL/MpJ-*Fas$^{lpr/lpr}$*.

479

480

References

1. Heredia JE, Mukundan L, Chen FM, Mueller AA, Deo RC, Locksley RM, Rando TA, Chawla A. Type 2 innate signals stimulate fibro/adipogenic progenitors to facilitate muscle regeneration. *Cell* 2013; **153**: 376–388.

2. Uezumi A, Fukada SI, Yamamoto N, Takeda S, Tsuchida K. Mesenchymal progenitors distinct from satellite cells contribute to ectopic fat cell formation in skeletal muscle. *Nature Cell Biology 2010 12:2* 2010; **12**: 143–152.

3. Joe AWB, Yi L, Natarajan A, le Grand F, So L, Wang J, Rudnicki MA, Rossi FMV. Muscle injury activates resident fibro/adipogenic progenitors that facilitate myogenesis. *Nat Cell Biol* 2010; **12**: 153–163.

4. Castiglioni A, Corna G, Rigamonti E, Basso V, Vezzoli M, Monno A, Almada AE, Mondino A, Wagers AJ, Manfredi AA, Rovere-Querini P. FOXP3+ T Cells Recruited to Sites of Sterile Skeletal Muscle Injury Regulate the Fate of Satellite Cells and Guide Effective Tissue Regeneration. *PLoS One* 2015; **10**: e0128094.

5. Chandra SR, Issac TG, Gayathri N, Shivaram S. Schwartz–Jampel syndrome. *J Pediatr Neurosci* 2015; **10**: 169–171.

6. Ieronimakis N, Hays A, Prasad A, Janebodin K, Duffield JS, Reyes M. PDGFRα signalling promotes fibrogenic responses in collagen-producing cells in Duchenne muscular dystrophy. *J Pathol* 2016; **240**: 410.

7. Schoenmaker T, Dahou Bouchankouk A, Özkan S, Gilijamse M, Bouvy-Berends E, Netelenbos C, Lobbezoo F, Eekhoff EMW, de Vries TJ. Limitations of Jaw Movement in Fibrodysplasia Ossificans Progressiva: A Review. *Front Med (Lausanne)* 2022; **9**: 852678.

8. Bach JF. The Effect of Infections on Susceptibility to Autoimmune and Allergic Diseases. *N Engl J Med.* 2002;**347**: 911–20.

9. Torres-Ruiz J, Alcalá-Carmona B, Alejandre-Aguilar R, Gómez-Martín D. Inflammatory myopathies and beyond: The dual role of neutrophils in muscle damage and regeneration. *Front Immunol* **2023**; 14: 1113214.

10. Hardy D, Besnard A, Latil M, Jouvion G, Briand D, Thépenier C, Pascal Q, Guguin A, Gayraud-Morel B, Cavaillon JM, Tajbakhsh S, Rocheteau P, Chrétien F. Comparative Study

510   of Injury Models for Studying Muscle Regeneration in Mice. *PLoS One* 2016; **11**: e0147198.

511 11.   Tidball JG, Villalta SA. Regulatory interactions between muscle and the immune system

512   during muscle regeneration. *Am J Physiol Regul Integr Comp Physiol* 2010; **298**: R1173–

513   R1187.

514 12.   Hawke TJ, Garry DJ. Myogenic satellite cells: Physiology to molecular biology. *J Appl*

515   *Physiol* 2001; **91**: 534–551.

516 13.   Seale P, Sabourin LA, Girgis-Gabardo A, Mansouri A, Gruss P, Rudnicki MA. Pax7 Is

517   Required for the Specification of Myogenic Satellite Cells. *Cell* 2000; **102**: 777–786.

518 14.   Mohamed AAA. Glycerol-induced injury as a new model of muscle regeneration. *Cell*

519   *Tissue Res* 2018; **374**: 233-241.

520 15.   Casciola-Rosen L, Nagaraju K, Plotz P, Wang K, Levine S, Gabrielson E, Corse A, Rosen

521   A. Enhanced autoantigen expression in regenerating muscle cells in idiopathic inflammatory

522   myopathy. *J Exp Med* 2005; **201**: 591.

523 16.   Sciorati C, Rigamonti E, Manfredi AA, Rovere-Querini P. Cell death, clearance and

524   immunity in the skeletal muscle. *Cell Death Differ* 2016; **23**: 927–937.

525 17.   Matsumoto K, Sakamoto Y, Hirose S. Granulocytosis and Its Correlation to

526   Lymphoproliferative Disorder in Autoimmune-prone MRL/lpr Mice. *Juntendo Medical*

527   *Journal* 1989; **35**: 106–116.

528 18.   Singer GG, Carrera AC, Marshak-Rothstein A, Martínez-A C, Abbas AK. Apoptosis, fas and

529   systemic autoimmunity: the MRL-Ipr/Ipr model. *Curr Opin Immunol* 1994; **6**: 913–920.

530 19.   Lemos DR, Babaeijandaghi F, Low M, Chang CK, Lee ST, Fiore D, Zhang RH, Natarajan

531   A, Nedospasov SA, Rossi FMV. Nilotinib reduces muscle fibrosis in chronic muscle injury

532   by promoting TNF-mediated apoptosis of fibro/adipogenic progenitors. *Nat Med* 2015; **21**:

533   786–794.

534 20.   Chikenji TS, Saito Y, Konari N, Nakano M, Mizue Y, Otani M, Fujimiya M. p16INK4A-

535   expressing mesenchymal stromal cells restore the senescence–clearance–regeneration

536   sequence that is impaired in chronic muscle inflammation. *EBioMedicine* 2019; **44**: 86–97.

537 21.   Garry DJ, Meeson A, Elterman J, Zhao Y, Yang P, Bassel-Duby R, Williams RS. Myogenic

538   stem cell function is impaired in mice lacking the forkhead/winged helix protein MNF. *Proc*

23

539   *Natl Acad Sci U S A* 2000; **97**: 5416–5421.

540   22.   Mohassel P, Rosen P, Casciola-Rosen L, Pak K, Mammen AL. Expression of the

541   Dermatomyositis Autoantigen TIF1γ in Regenerating Muscle. *Arthritis Rheumatol* 2015; **67**:

542   266.

543   23.   Liu L, Akkoyunlu M. Circulating CD138 enhances disease progression by augmenting

544   autoreactive antibody production in a mouse model of systemic lupus erythematosus. *J Biol*

545   *Chem* 2021; **297**: 101053.

546   24.   Cholok D, Lee E, Lisiecki J, Agarwal S, Loder S, Ranganathan K, Qureshi AT, Davis TA,

547   Levi B. Traumatic muscle fibrosis: From pathway to prevention. *J Trauma Acute Care Surg*

548   2017; **82**: 174–184.

549   25.   Lieber RL, Ward SR. Cellular Mechanisms of Tissue Fibrosis. 4. Structural and functional

550   consequences of skeletal muscle fibrosis. *Am J Physiol Cell Physiol* 2013; **305**: C241-252.
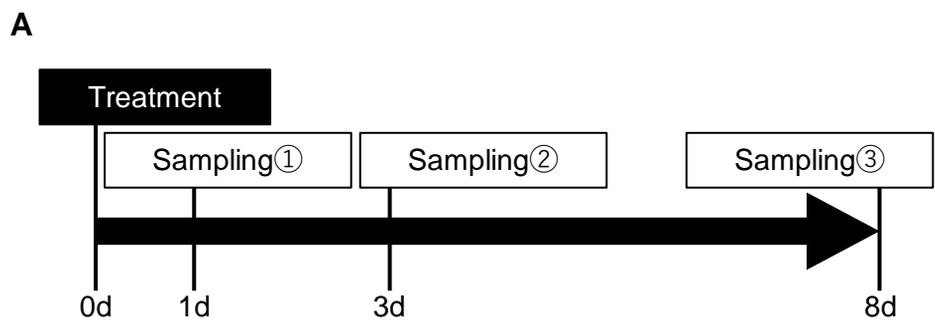
551

Figure 1

A

Treatment

| Sampling① | Sampling② | Sampling③ |

0d   1d   3d   8d

B **Anti-dsDNA**
☐MpJ ■lpr

U/mL

10,000
1,000
100
10
1

1d   3d   8d

C **SPW/BW ratio**
☐MpJ ■lpr

%

3.0
2.0
1.0
0.0

1d   3d   8d
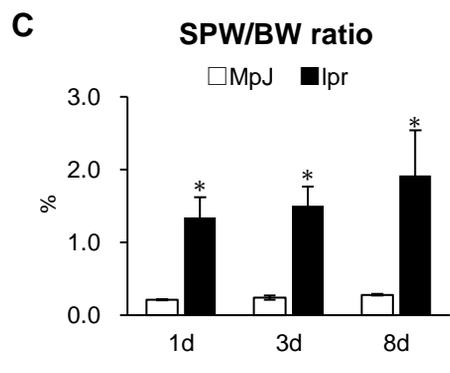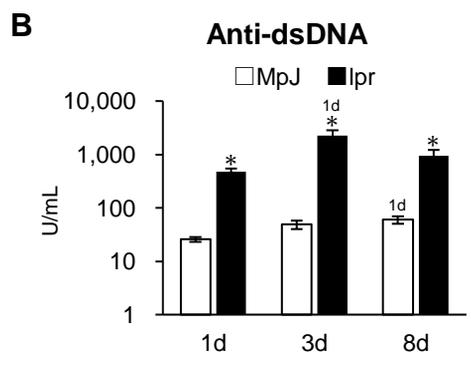
Figure 2

Figure 3

Figure 4

A

| | 1d | 3d | 8d |

B220 / MpJ

B220 / lpr

B

| | 1d | 3d | 8d |

CD3 / MpJ

CD3 / lpr

C
B220

P = 0.063

□MpJ ■lpr

Positive / All

1d 3d 8d

D
CD3

*

□MpJ ■lpr

Positive / All

1d 3d 8d

Figure 5

A — BrdU — 1d / 3d / 8d — MpJ / lpr

B — BrdU — Incorporation / All (%) — $P = 0.095$, $P = 0.053$ — 1d / 3d / 8d — □MpJ ■lpr

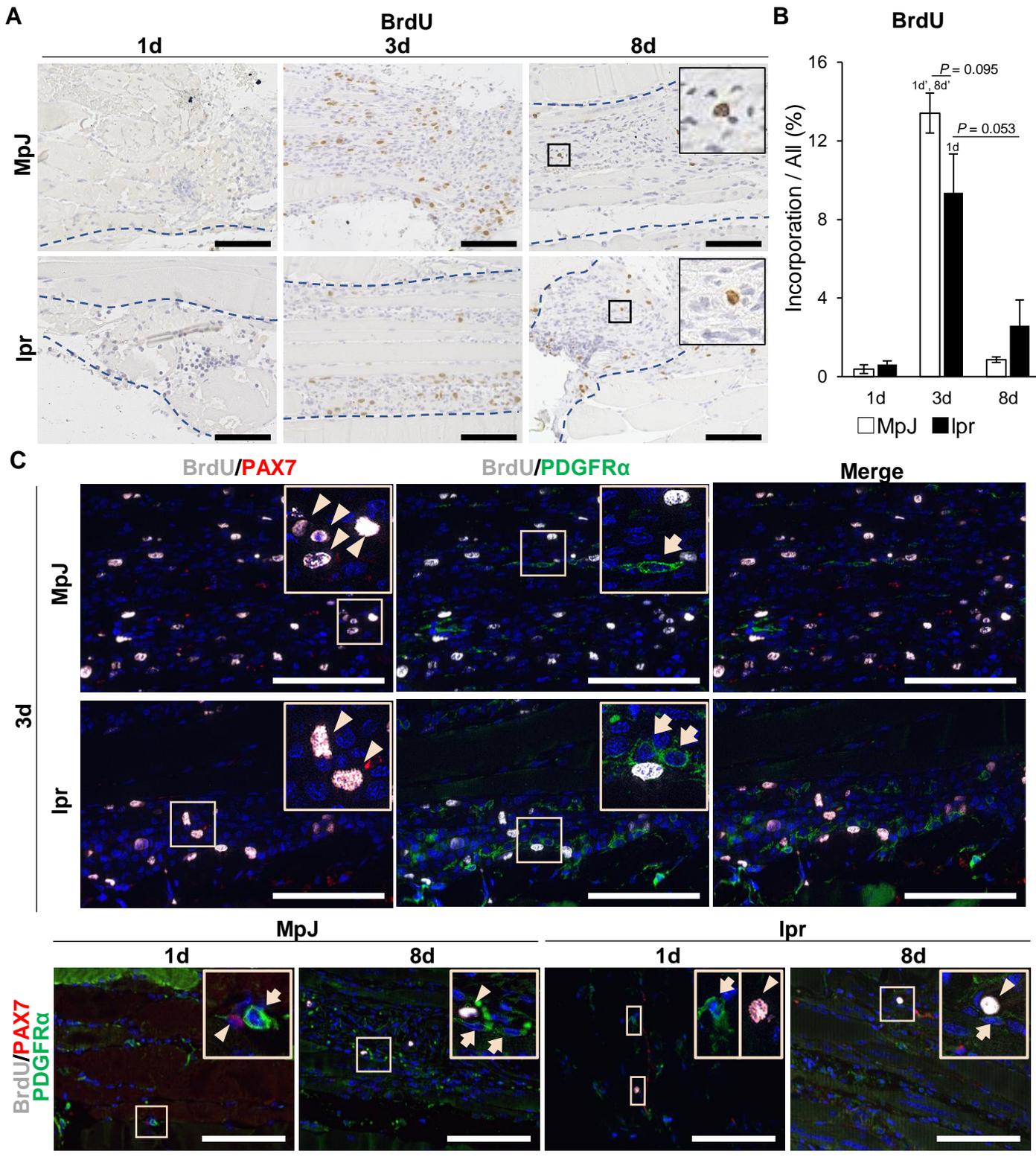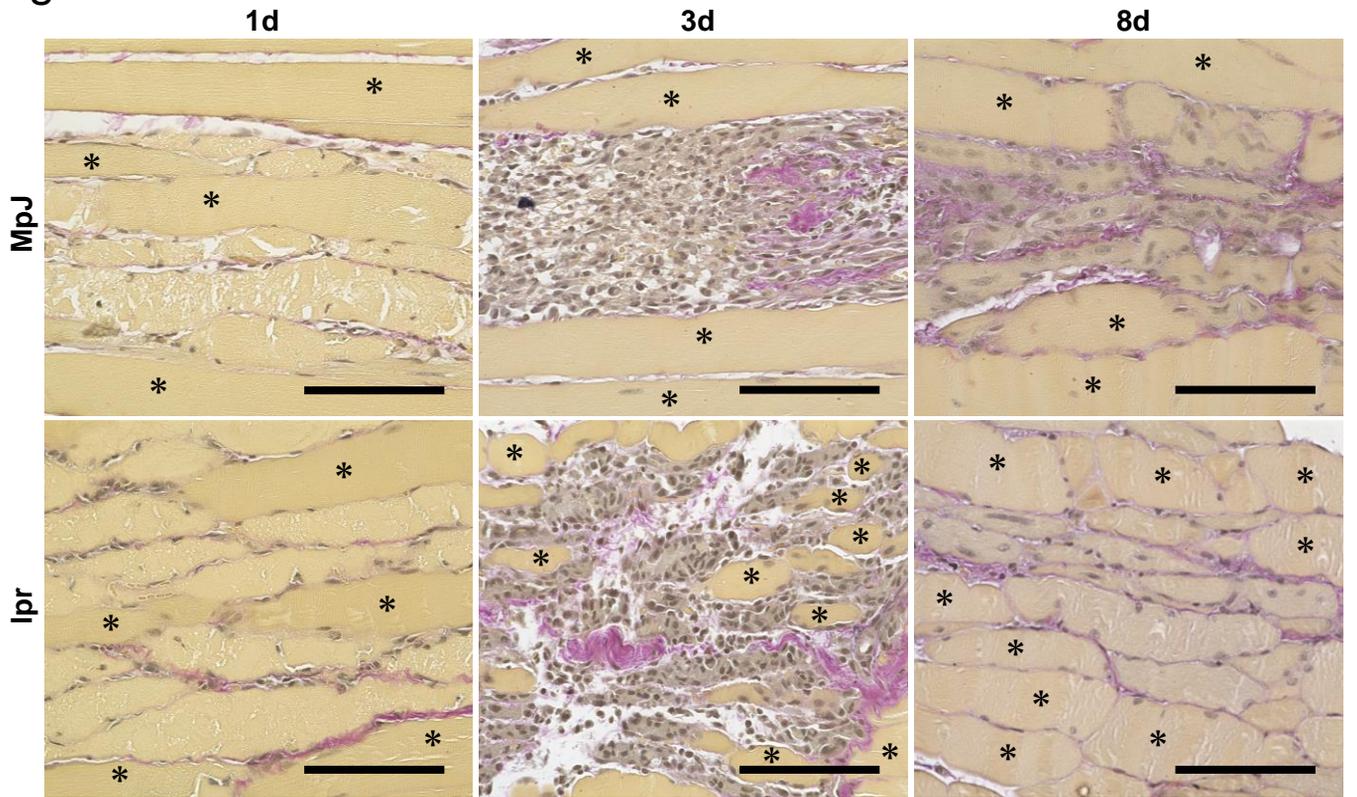**C** — BrdU/PAX7 — BrdU/PDGFRα — Merge — MpJ / lpr — 3d

MpJ — 1d / 8d — lpr — 1d / 8d — BrdU/PAX7/PDGFRα
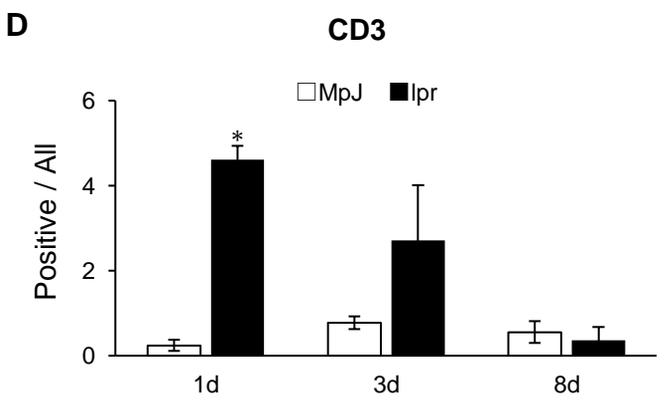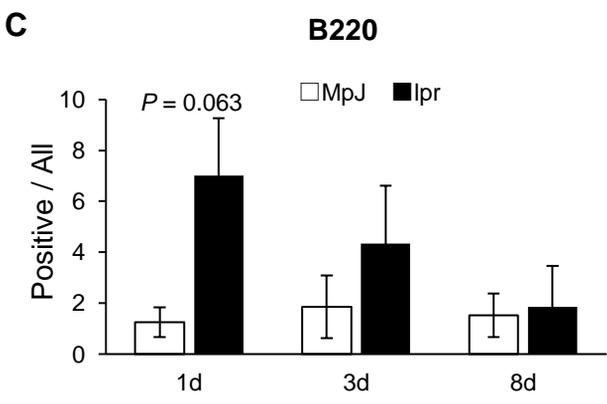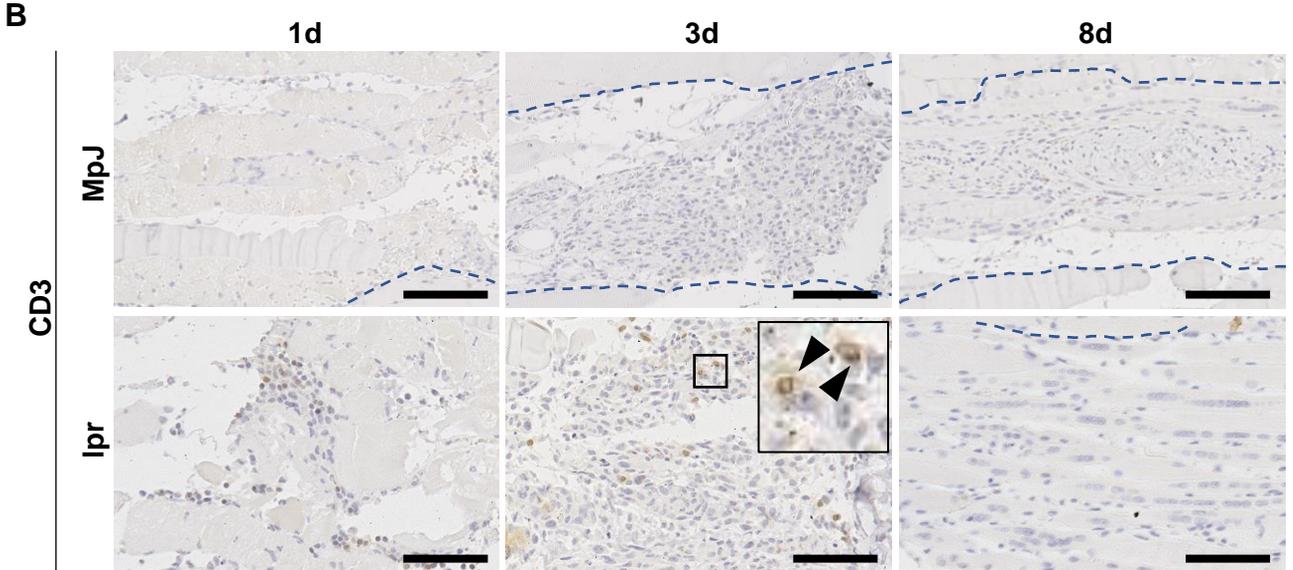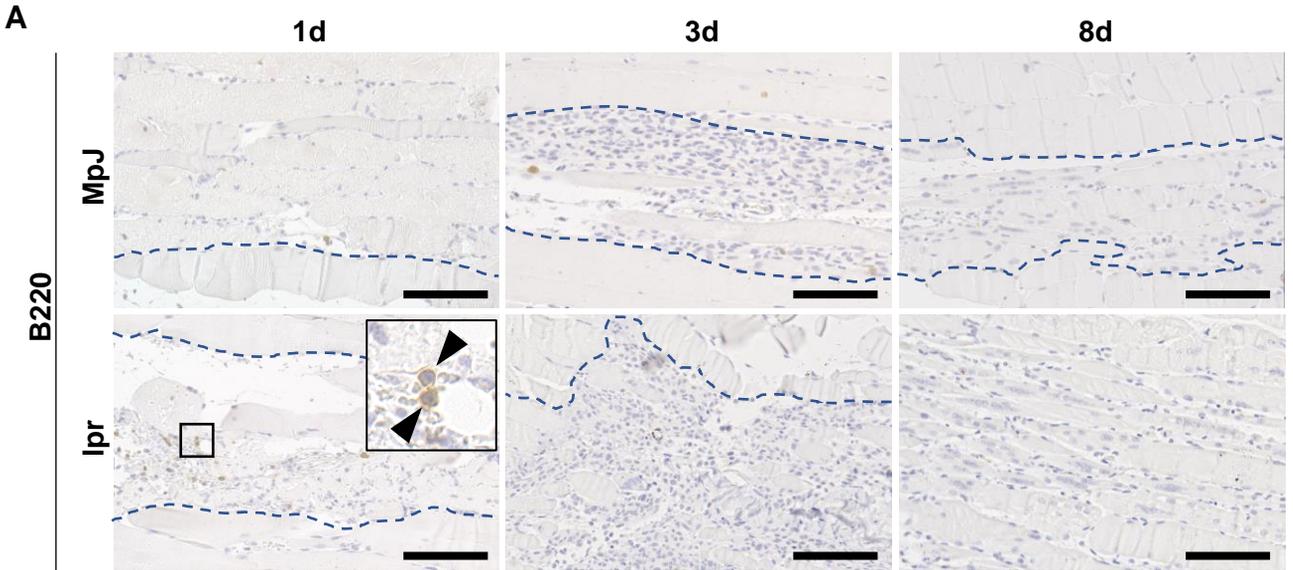
Figure 6

Supplemental figure 1